JOURNAL OF PROPULSION AND POWER
Vol. 15, No. 5, September–October 1999

Shock-Tunnel Skin-Friction Measurement in a Supersonic Combustor

C. P. Goyne,* R. J. Stalker,† and A. Paull‡
University of Queensland, Brisbane, Queensland 4072, Australia

Shock-tunnel measurements are reported of skin friction with supersonic hydrogen–air combustion in a constant area duct. A floating-element skin-friction gauge was used, in which the shear force was applied directly to a piezoceramic measuring element. The experiments were conducted at stagnation enthalpies of 5.7 and 6.8 MJ kg^{-1}, a precombustion Mach number of ~4.5, and with a maximum duct Reynolds number of 1.3×10^7. The measurements showed that, although supersonic combustion caused the skin friction to fluctuate with time, it did not affect the mean value of the skin-friction coefficient, and this mean value could be predicted using existing turbulent boundary-layer theory. Measurements of heat transfer also established that Reynolds analogy could be used in both the fuel-off and fuel-on flows.

Nomenclature

c_f = skin-friction coefficient
c_h = Stanton number
c_p = specific heat at constant pressure
n = number of measurements
Pr = Prandtl number
$\dot{q}$ = heat transfer rate
r = $\tau/\dot{q}$
T = mainstream temperature
T_w = wall temperature
t = student's t
U = mainstream velocity
ΔH = $c_p(T - T_w) + 0.44\,U^2$
ρ = mainstream density
σ = standard deviation
τ = skin friction

Subscripts

n = fuel-off
0 = fuel-on

Introduction

AIR-BREATHING propulsion is accomplished by producing thrust that equals or exceeds the drag on a vehicle. Thrust is generated by adding energy to the airstream, in the form of heat, and converting it into thrust work. Because heat addition is invariably effected by combustion, it is limited by the calorific value of the fuel, which is independent of flight speed. And, as the work done by a given level of thrust increases with the flight speed, it follows that the thrust tends to decrease with increasing flight speed. On the other hand, the skin-friction drag depends on the square of the flight speed. The well-known consequence of this is that skin-friction drag must become an increasingly significant fraction of the propulsive balance of forces as the flight speed increases.

An important part of the skin-friction drag is contributed by supersonic combustors. This is illustrated by experiments with an axisymmetric integrated scramjet configuration, using constant area combustors,[1] at freestream velocities between 2.2 and 3.6 km s^{-1}. Calculations indicated that combustion chamber skin friction contributed ~28% of the total drag, and 60% of the overall skin friction drag. The maximum net thrust in the experiments was obtained at 2.2 km s^{-1}, and was only half of the calculated skin friction in the combustion chambers. Although the choice of theory on which the calculations of skin friction were based could lead to a difference in the values obtained exceeding 40%, the investigation served to demonstrate the influence of combustion chamber skin friction on net thrust. The fact that this influence will grow with flight speed, and that uncertainty exists regarding the theoretical predictions, makes it desirable that combustion chamber skin friction be measured at high speeds.

Impulse facilities, such as the shock tunnel or the expansion tube,[2] offer the only practical means of generating flows at the necessary speeds. The shock tunnel offers longer test times than the expansion tube, and, therefore, is able to accept larger models, but both have been used previously for measurements of skin friction.[3–6]

Early shock-tunnel measurements of skin friction were reported by Holden.[3] The gauge consisted of a floating element supported by two cantilever piezoceramic beams that developed a charge when deflected. Measurements were obtained on a flat plate at flow velocities up to 2.4 km s^{-1}. More recently, Bowersox et al.[7] have developed a gauge with the floating element supported by a single cantilever beam. The beam was instrumented with semiconductor strain gauges. Novean et al.[6] tested an improved version of this gauge in a combustion duct in an expansion tube, with mixed success.

As a means of obtaining a higher-frequency response than had been achieved with cantilever beam-type gauges, Kelly et al.[8] designed a skin-friction gauge that employed direct shear of a piezoceramic measuring element. The gauge was used to measure laminar skin friction in a small free-piston shock tunnel. With subsequent modification and development, this type of gauge has been used to measure turbulent skin friction in a free-piston shock tunnel.[4,5] The present experiments utilize this type of skin-friction gauge. Simultaneous measurements were made of the distributions of skin friction, heat transfer, and pressure along the length of a rectangular, constant area, combustion duct. The precombustion airflow Mach number was 4.5, and the fuel was hydrogen, whereas the maximum stagnation enthalpy corresponded to a flight velocity of 3.6 km s^{-1}. The use of a constant-area duct of a moderately high precombustion Mach number ensured that, in spite of the combustion pressure rise, changes in the density and the velocity along the duct were small (of the order of a few percent). This simplified interpretation of the results.

This paper begins by describing the experimental apparatus, with emphasis on the skin-friction gauges. The skin-friction

Received 10 November 1997; presented as Paper 98-0943 at the AIAA 36th Aerospace Sciences Meeting and Exhibit, Reno, NV, 12–15 January 1998; revision received 15 December 1998; accepted for publication 6 January 1999. Copyright ©1999 by the American Institute of Aeronautics and Astronautics, Inc. All rights reserved.

*Postgraduate Scholar, Department of Mechanical Engineering. Student Member AIAA.
†Emeritus Professor, Department of Mechanical Engineering. Associate Fellow AIAA.
‡Senior Research Fellow, Department of Mechanical Engineering.

Table 1 Test conditions—Airflow

Quantity	Units	Estimated error, %	Conditions 1	Conditions 2
Stagnation enthalpy	MJ kg^{-1}	+4, −8	6.8	5.7
Nozzle reservoir pressure	MPa	±5	34	30
Mach number	——	——	4.4	4.5
Precombustion temperature	K	−4, −8	1370	1100
Precombustion pressure	kPa	±8	78	64
Precombustion density	kg m^{-3}	±13	0.198	0.202
Precombustion velocity	ms^{-1}	+2, −4	3160	2930
Reynolds number per m	m^{-1}	——	1.2×10^7	1.3×10^7
Equivalence ratio	——	±16	0.9	1.0

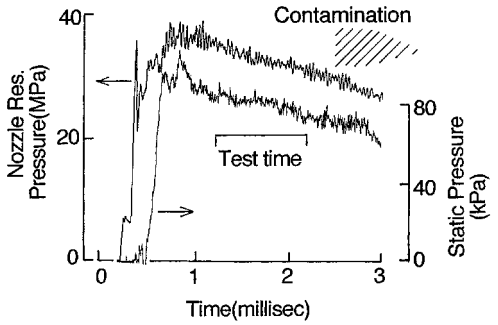

Fig. 1 Typical test pressure records.

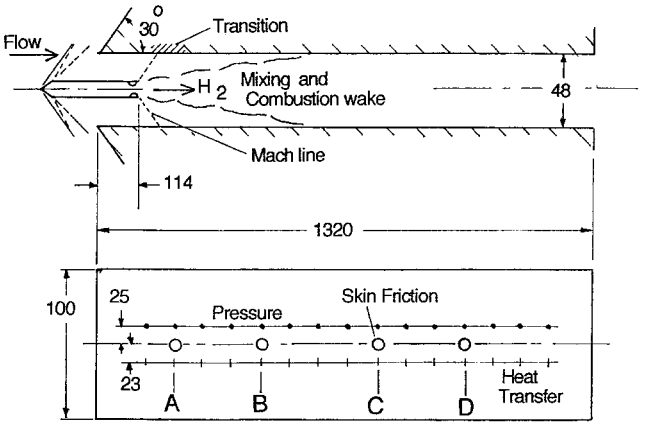

Fig. 2 Experimental duct (dimensions in millimeters).

measurement technique is outlined, and the results are then presented and discussed, before leading to the Conclusions.

Experiment

Shock Tunnel and Test Conditions

The experiments were conducted in the shock reflected T4 free-piston shock tunnel at the University of Queensland. The shock tunnel is described elsewhere.[1,9] Basically, it consisted of a free-piston driver, 229 mm in diameter and 26 m long, with a shock tube 75 mm in diameter and 10 m long. The shock tube supplied a contoured axisymmetric nozzle of 25 mm throat diameter and 135 mm exit diameter. After expansion through the nozzle, the test flow passed directly into the experimental duct, and therefore, the experiments were essentially of the "direct connect" type.

The test conditions are set out in Table 1. The nozzle stagnation enthalpy was obtained from the shock speed and the initial pressure in the shock tube. Where necessary, isentropic expansion of the air in the reflected shock region to the measured nozzle reservoir pressure was also invoked. A numerical calculation of the nonequilibrium nozzle expansion then yielded the test flow conditions.[9,10]

Typical records of nozzle reservoir pressure and the static pressure at the first transducer in the experimental duct are presented in Fig. 1. The test period is also shown, and corresponds to the time taken for the airflow to pass a distance equal to three times the instrumented length of the duct. The test conditions are taken as the mean value over the test period. The time when the airflow may be contaminated by the helium–argon driver gas[11] is also displayed.

Experimental Duct

The experimental duct is shown in Fig. 2. Note that the longitudinal dimensions are scaled by a factor of 4 relative to lateral dimensions in order to display detail more clearly. The duct is of 48×100 mm rectangular cross section, with a fuel-injection strut 10 mm thick, which spans the 100 mm dimension in the midplane of the duct. The leading edge of the strut is located sufficiently far upstream to ensure that the shocks and expansion waves that it creates do not enter the duct. Hydrogen is injected from a nozzle spanning the blunt trailing edge of the strut. The approximate boundaries of the resulting mixing and combustion wake, as determined from previous experiments,[12] are also shown, and it can be seen that it fills the duct from ~500 mm downstream of the injection station. If the boundary layers on the walls of the duct are taken into account, the wake fills the duct from an even shorter distance downstream of the injection station. This is also confirmed by optical studies of a combustion duct that was a half-scale version of the present one.[13]

Previous experiments in the shock tunnel[14] indicate that transition of the boundary layers will be expected within 150 mm of the duct leading edge, as shown in Fig. 2, and therefore, the boundary layers are turbulent over most of the duct length. The estimated boundary-layer displacement thickness 500 mm downstream of injection is 1.5 mm. As shown, one wall of the duct was instrumented with skin-friction gauges, thin film heat transfer gauges, and PCB piezotronic piezoelectric pressure transducers.

Hydrogen fuel was introduced from a room-temperature reservoir through a solenoid-operated valve that was triggered by recoil of the shock-tunnel assembly prior to arrival of the test flow. The hydrogen was supplied to each of the two ends of the injection strut through two supply ducts, and the pressure in each was monitored by a piezoelectric transducer. The supply pressure was constant throughout the test time. Injection took place through a two-dimensional supersonic nozzle with a 1.6 mm throat, and after isentropic expansion to the precombustion static pressure, the hydrogen Mach number and velocity was 2.2 and 2000 ms^{-1}, respectively. The system was precalibrated to yield the mass flow of hydrogen from the measured supply pressure.

Skin-Friction Gauges

The principle of operation of the gauges used is shown in Fig. 3a. The skin-friction force is applied through a floating element that is attached directly to a piezoceramic ring. The piezoceramic material is lead zirconate titanate, PZT-5H, supplied by Morgan Matroc, of Southampton, England, United Kingdom. The gauge is mounted so that the direction of polarization of the piezoceramic is parallel to the direction of the skin-friction force to be measured. In principle, the piezoceramic is therefore sensitive only to a shear force, and not to the normal force arising from the flow static pressure acting on the floating element. However, manufacturing tolerances allow a

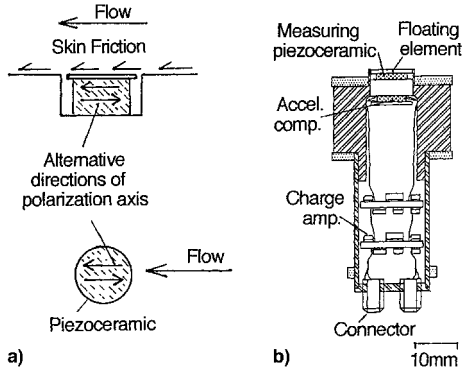

Fig. 3 Skin-friction gauge: a) principle of operation and b) design layout.

residual pressure effect, but this can be accounted for in the manner described next.

The design of the gauges is shown in Fig. 3b. It incorporated a measuring- and an acceleration-compensating piezoceramic. Both consisted of a 1.5-mm-thick, 8-mm-diam PZT-5H ring with a 2-mm-hole through the center. The ceramics were located on each side of an aluminium base and 10-mm-diam invar disks were joined to each of the two remaining faces. One of these invar disks formed the skin-friction sensing surface, whereas the other, protected from the flow, was used for acceleration compensation. Both ceramics were covered by an acrylic insulator that was then coated with a conductive paint. The coating was earthed and acted as an electric shield. The sensing ceramic was also wrapped in approximately 11 layers of fine brass mesh. This acted to cool the freestream air that entered the cavity formed between the piezoceramic-invar assembly and the brass gauge housing. The design resulted in a lowest natural frequency of ~40 kHz.

The transducers were calibrated for transient shear and acceleration forces in separate bench tests. Transient pressure calibration was obtained in situ, within the shock-tunnel flow, using the wall static pressures measured adjacent to each transducer.

Shear calibrations were obtained by loading the sensing element using an adhered cotton thread arrangement. A vertically hung weight, of known mass, was suddenly released to produce a step change in applied force with a rise time of less than 1.5 ms. Figure 4a presents a typical shear calibration.

Acceleration calibrations were obtained by vibrationally exciting the gauge, along the sensing axis, using an electrodynamic vibrator. Determination of the ratio of measuring element output to acceleration element output permitted routine subtraction of the acceleration component of the signal during service. A nominal excitation frequency of 300 Hz was used, to approximately match the predicted dominant frequency of acceleration experienced by the gauge in the shock tunnel. A check measured at 1 kHz was also obtained. Figure 4b presents a typical acceleration calibration.

Pressure calibrations were obtained through a series of paired shock-tunnel runs. Measurements were obtained for one test condition and then repeated with the skin-friction gauge rotated by 180 deg relative to the flow. The shear component of the gauge output changed sign with rotation, but the pressure component did not. By comparing half the sum of the two signals with the average static pressure measured adjacent to the gauge, the pressure sensitivity of the transducer was established. Figure 4c presents a typical pressure calibration. During the tests conducted here, the pressure components of the gauge output represented about 30% of the shear component.

Pressure and Heat Transfer

As shown in Fig. 2, static pressure was measured with PCB piezotronic piezoelectric pressure transducers located on the same wall of the duct as the skin-friction gauges. Heat transfer was also measured on the same wall using platinum thin film heat transfer gauges mounted on a quartz substrate. Because of the geometry of

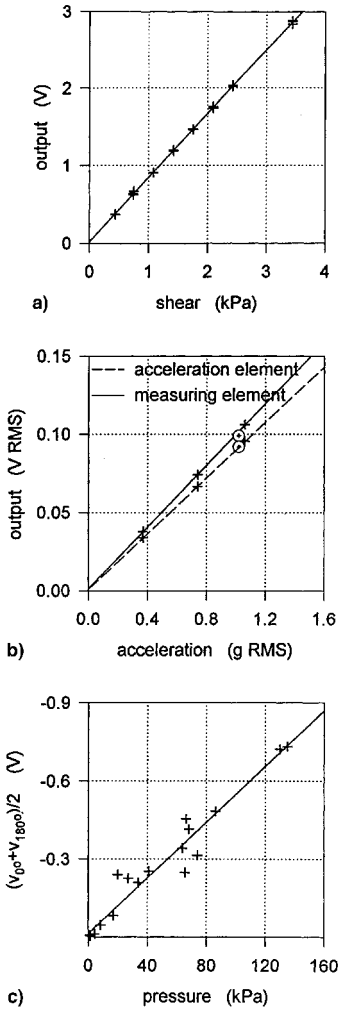

Fig. 4 Example of calibration for a skin-friction gauge: a) shear, b) acceleration 300 Hz (circles 1 kHz), and c) pressure.

the duct and injection system, the flows produced were essentially two dimensional, and, therefore, the measurements of pressure and heat transfer by the gauges adjacent to the skin-friction gauges were taken to apply at the location of the skin-friction gauges.

Data Recording

Data were recorded and stored on a 12-bit transient digital data store with a sampling time of one μs. The output from the skin-friction gauges was recorded directly, whereas the output from the pressure transducers and the heat transfer gauges was recorded through 4 × multiplexers, resulting in a sampling time of 4 μs for each channel. The recorded signal from the pressure transducers was time averaged over a period of 20 μs before display, whereas the signals from the thin film heat transfer gauges were computer processed to display the heat transfer rate. Because of the high heat transfer rates experienced, it was necessary to take account of the change in properties of the quartz substrate in processing the signal.[15]

Results and Discussion

Skin-Friction Records

A typical set of skin-friction records is shown in Fig. 5. The records are arranged according to the station of the gauge in the duct. It will be observed that the upstream gauge shows a temporary reduction in the skin friction during the approach to a steady value, and that, in passing to successive gauges, this reduction grows into a strong reversal of the skin friction. The nature of the flow starting process in the hypersonic nozzle and the resulting flow through the duct explains this effect. As shown in Fig. 6, the starting flow in

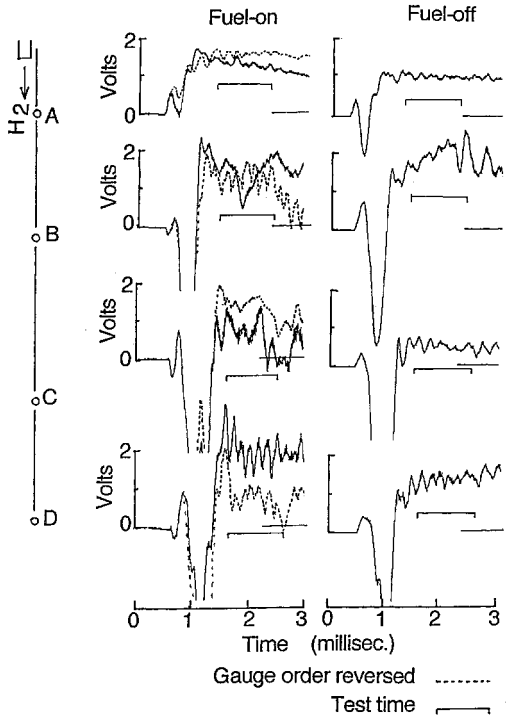

Fig. 5 Typical skin-friction records (condition 1).

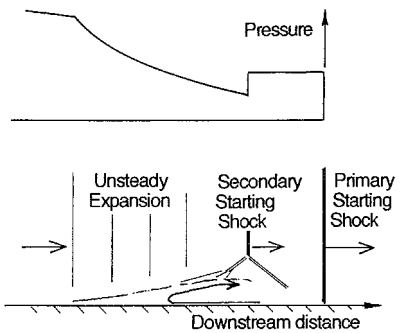

Fig. 6 Duct starting flow.

the nozzle leads to formation of a primary starting shock, followed by a secondary starting shock and an unsteady expansion.[16] The secondary starting shock faces upstream, but is swept downstream, along with the rest of the starting wave system. When the starting wave system enters the duct, the secondary starting shock causes a region of separated flow to develop as it passes down the duct, and hence, a reversal in the skin friction. The duct starting process is completed when this separation region is swept from the duct, and steady flow ensues.

The separated region experiences an increase in pressure as the unsteady expansion is swept downstream. The resulting increase in density causes the separated region to become thinner, velocity gradients normal to the surface are increased, and hence, the skin friction increases. This effect may be expected to lead to larger magnitudes of skin-friction reversal when the pressure change across the unsteady expansion is increased. This occurs for instance during the nozzle starting process when the ratio of nozzle reservoir pressure to initial test section pressure is increased. Tests where this ratio was varied showed that the magnitude of the skin-friction reversal did indeed vary as expected, and therefore, provided qualitative confirmation of the proposed mechanism of skin-friction reversal.

The skin-friction records of Fig. 5 are time averaged over 100 μs, and are records of the acceleration-compensated gauge output, before the pressure sensitivity and the shear calibration factors have been taken into account. Two sets of fuel-on records are presented, the second set corresponding to the gauges being relocated in reverse order in the duct; i.e., the gauges that were at stations A and B were exchanged with those located, respectively, at stations D and C. This was done to avoid the possibility of mistaking the response characteristics of a particular gauge for a feature of the flow.

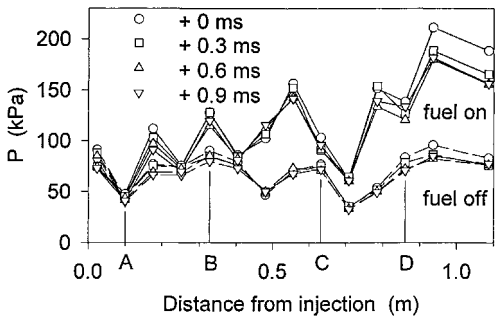

Fig. 7 Typical pressure distributions (condition 1).

Station A is close to the point at which the Mach line from the trailing edge of the injection strut strikes the surface and yields gauge outputs, which, after passage of the separated region, are relatively steady during the test time. These are typical of outputs obtained in previous measurements of skin friction on a flat plate in a rectangular duct,[4,5] and is the output expected when measuring skin friction in a steady flow. For the fuel-on flows, the outputs at the remaining stations exhibit apparently random fluctuations during the test time, whereas for the fuel-off case these are confined to station B, with station D exhibiting a tendency for the output to slightly increase with time.

These random fluctuations are ascribed to shocks and expansion waves, arising from the presence of the injection strut and from the combustion wake, giving rise to local regions of pressure gradient along the surface. Figure 7 shows typical duct unaveraged pressure distributions, taken at 0.3-ms intervals during the test time, for both fuel-on and fuel-off cases. Although the pressure gradients are not captured in detail, the pressure distributions show that substantial streamwise variations in pressure exist, and that these are greater for the fuel-on cases than for the fuel-off case. The pressure distributions vary by only a small amount with time, but in the vicinity of strong pressure gradients, a small shift in the pressure distribution can correspond to a substantial change in the pressure gradient at a point, and, therefore, it is necessary to consider the effect these pressure gradients may have on the skin-friction gauges.

While other investigators have found that skin-friction gauges are sensitive to pressure gradients,[6] this sensitivity is reduced with the present gauges. A pressure gradient across the floating element of the gauge will have two effects. One effect is to apply a moment to the floating element, and the other is to apply a lip force, acting in the shear-sensing plane of the element, due to the distribution of pressure on the lip face of the floating element. In regard to the former effect it is noted that, in principle, piezoceramics operated in the shear mode are inherently insensitive to moments. To check this a 10-mm-diam flange, with a 16-mm-long, 2-mm-diam post attached, was temporarily adhered to the floating element of each of the gauges, with the post aligned with the axis of symmetry of the gauge. This arrangement was used to apply a calibrating shear force to the gauge, together with a moment that could be varied by changing the point on the post at which the force was applied. The results showed that, for the pressure gradients of Fig. 7, the moment effect would alter the measured shear stress by 3% or less. The possible error due to the lip force can be much greater than that. Taking the lip force as the product of the pressure gradient, the lip thickness (0.8 mm), and half the area of the floating element,[17] it is found that for the pressure gradients of Fig. 7 the lip force can correspond to as much as 25% of the measured shear force.

The fluctuations in gauge output seen in Fig. 5 indicate skin-friction variations that are considerably greater than 25%, and it is concluded that a major part of these fluctuations must be due to variations in the local skin friction in the flow. It is noted that, with the exception of station A, these fluctuations in skin-friction are

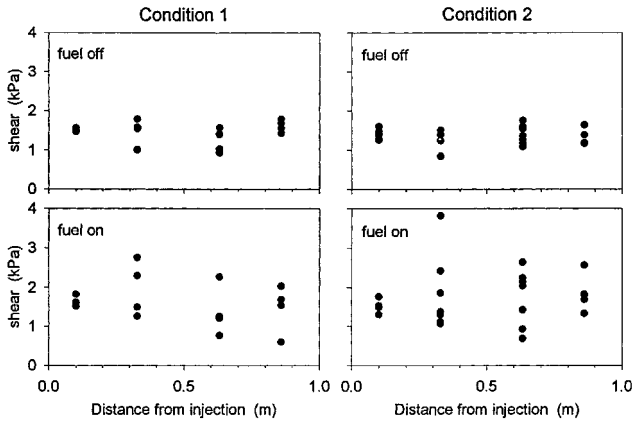

Fig. 8 Skin-friction measurements.

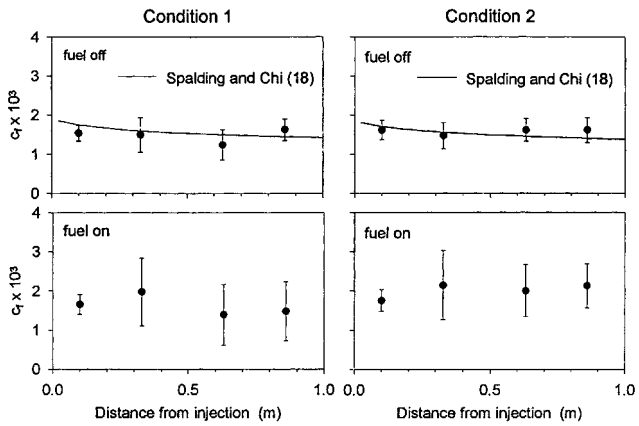

Fig. 9 Skin-friction coefficient.

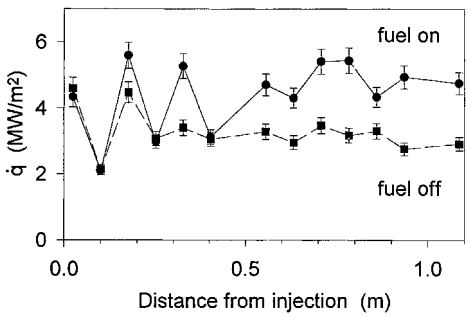

Fig. 10 Typical heat transfer distributions (condition 1).

greater for the fuel-on cases, which is consistent with the turbulent combustion wake being their primary source. Thus, the skin-friction records are the response of the gauges to the variations of skin friction in the flow itself, as well as a limited response to the pressure gradients that occur in the flow. This pressure gradient effect on the gauges is due mainly to local variations in the pressure gradient, and will be discussed next. The mean duct fuel-on pressure gradient is only expected to introduce an error in the gauge measurement of ~3%.

Measurements were made by averaging the output of the skin-friction gauges over the test time, and taking the pressure sensitivity and the shear calibration factor into account. The results are shown in Fig. 8, for both test condition 1 and test condition 2. Test condition 2 involved a lower precombustion temperature than 1, thereby changing combustion rates. Thus, although the overall pressure distributions were similar to those at condition 1, they differed in the detailed location of pressure peaks and troughs, and therefore, would be expected to yield different varying pressure gradients. This served to eliminate the possibility that the fluctuations in gauge output were a special feature of test condition 1.

It can be seen that, for both conditions, the gauges at station A yielded consistent results but, with the exception of station D for the fuel-off cases, the disturbances in the flow gave rise to considerable scatter in the measured values of the skin-friction shear stress at the remaining stations. The scatter is somewhat greater for the fuel-on case at condition 2 than at condition 1, which is consistent with the fact that greater timewise fluctuations in the pressure distributions were observed at condition 2.

The effect of lip forces due to local pressure gradients was obtained approximately from Fig. 7, which displays pressure gradients representative of the experiments. Though the spacing of the pressure transducers did not allow the pressure gradients to be captured in detail, approximate estimates could be derived as the mean of the upstream and downstream gradients at each skin-friction gauge station. These estimates were used to obtain the lip forces for the fuel-on case. Taking the pressure gradient as positive for pressure increasing in the streamwise direction, the lip force was −4, +2, +16, and −9% of the mean value of the measured shear forced at each of stations A, B, C, and D, respectively. In view of the scatter in the measured value of shear stress seen in Fig. 8, and the variation in the direction of the lip force from station to station, it was concluded that the effect of the lip force on the measured average of shear stress in the duct was negligible. Thus, notwithstanding the fact that the lip force had a relatively small, systematic effect at each skin-friction gauge, no attempt was made to isolate this effect in the measurements presented.

Thus, the mean value of the measurements at each station was taken as the shear stress there. The skin-friction coefficient

$$c_f = 2\tau/(\rho U^2) \tag{1}$$

could then be obtained from the mean value of the measurements of shear stress at each station following referral to Table 1 for the precombustion stream properties. The resulting values are plotted in Fig. 9. The error bars are calculated by treating the measured values of shear stress as a normally distributed sample, thereby yielding the confidence interval for the mean as $t\sigma/\sqrt{n}$ where σ is the standard deviation of n measurements and t is Student's t for a 90% confidence interval with $(n-1)$ degrees of freedom. The rss combination of this value with a 12% gauge calibration bias error and a 2% error in ρU^2 results in the error bars shown. As expected, the error bars are largest in the fuel-on cases.

It can be seen in Fig. 9 that the mean values of skin-friction coefficient exhibit little variation in passing along the duct from station A into the combustion region, and that the fuel-on values are not significantly different from the fuel-off values. Figure 9 also shows that the fuel-off values are consistent with predictions based on experiments by other investigators at lower stagnation enthalpies[18] with a cold surface. These results lead to the conclusion that the time average of skin friction is not significantly altered by supersonic combustion.

Heat Transfer

Typical heat transfer distributions are presented in Fig. 10. The fuel-on case shows a substantial increase in heat transfer with distance along the duct as combustion takes place. This is different to the observed skin-friction behavior. Order of magnitude estimates pointed to the possibility that the skin friction may have been reduced by the rise in pressure along the duct, and so this was explored numerically. A two-dimensional model of the duct flow was used, and an isentropic compression was applied along the duct. A space marching, parabolized Navier–Stokes finite volume code was used that incorporated a Baldwin–Lomax turbulence model with a compressibility correction.[19] An exponential grid refinement at the duct surface ensured that the behavior of the boundary layer at the surface was captured. Resulting distributions of pressure, heat transfer and skin friction are displayed in Fig. 11. The heat transfer and skin friction follow almost identical curves, showing that the effect of applying a pressure gradient alone to the surface as a compression wave in an isentropic flow does not explain the experimental observations.

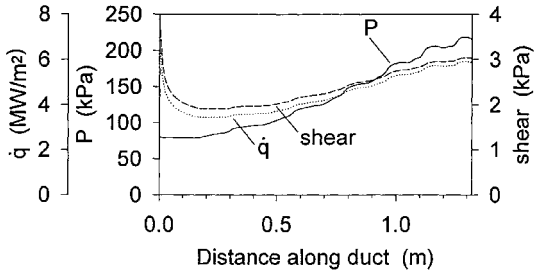

Fig. 11 Calculated effect of pressure gradient on skin friction and heat transfer.

This led to the following discussion on Reynolds analogy in flows with supersonic combustion.

Reynolds Analogy

Reynolds analogy involves the relation between heat transfer and skin friction, and to investigate this it is noted that the heat transfer is given by

$$\dot{q} = c_h \rho U \Delta H \tag{2}$$

where $\Delta H = c_p(T - T_w) + 0.44U^2$ for a turbulent boundary layer,[20] and $T_w = 300$ K is taken as the temperature at the surface of the duct. Combining this with Eq. (1), the ratio of skin friction to heat transfer rate can be written as

$$r = \tau/\dot{q} = 0.5(U/\Delta H)c_f/c_h \tag{3}$$

and therefore

$$\frac{r_0}{r_n} = \frac{R(c_f/c_h)_0}{(c_f/c_h)_n} \tag{4}$$

where $R = (U/\Delta H)_0/(U/\Delta H)_n$. These relations are used in the analysis of experimental results that follows.

First, the skin-friction measurement was divided by the heat transfer measurement, obtained with the heat transfer gauge adjacent to the skin-friction gauge, to produce a value of r at each skin-friction gauge station for each run. In the absence of fuel addition, the mean characteristics of the duct boundary layer may be represented by a turbulent boundary layer on a flat plate in air, implying that Reynolds analogy applies, and therefore[20]

$$c_f/c_h \approx 2Pr^{\frac{2}{3}} = 1.61 \tag{5}$$

This was checked by using the mean of the measured value of r, together with Eq. (3), to obtain values for c_f/c_h of 1.7 ± 0.2 and 1.8 ± 0.3 for conditions 1 and 2, respectively, the errors representing uncertainties in the calibration of skin friction and heat transfer gauges. Thus, to within experimental errors, Reynolds analogy applies to the fuel-off flows.

Next, each fuel-on value of r was divided by each fuel-off value at each station, and the mean of all the resulting values at each station was taken, to yield the results presented in Fig. 12. The error bars represent the 90% confidence limit, obtained as for Fig. 9. The variation of R along the duct is calculated by noting that, as shown in Fig. 2, the mixing and combustion wake fills the duct from a station less than 500 mm downstream of the injection station, suggesting that the mainstream in the duct be modeled as a one-dimensional flow, with combustion represented by heat addition uniformly across the duct.

Thus, the variation of stagnation enthalpy and velocity along the duct was determined by a Rayleigh flow analysis, with a ratio of specific heats of 1.3, the mean precombustion static pressure of conditions 1 and 2, and with the pressure rise along the duct taken as a uniform pressure gradient of 140 kPa m^{-1}. The resulting variation of R is also represented in Fig. 12. It can be seen that the trend of the measurements follows that for R, and referring to Eq. (4), that c_f/c_h is unchanged in passing from the fuel-off to the fuel-on case. Thus, Reynolds analogy also applies in the combustion region, and

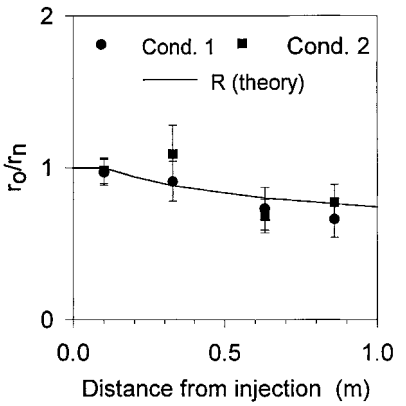

Fig. 12 Reynolds analogy—effect of combustion.

therefore, the observed increase in fuel-on heat transfer, without a corresponding increase in skin friction, can be ascribed to the change in main stream properties.

Conclusions

Skin-friction measurements have been made in a supersonic, hydrogen–air combustion flow in a constant area duct with turbulent boundary layers. The measurements were performed in a shock tunnel using a floating element gauge, which employed direct shear of the piezoceramic element.

The experiments illustrated the difficulties involved in making skin-friction measurements in a supersonic combustion region. The shocks and expansion waves generated by the combustion process, and by the method of introducing fuel, led to random disturbances in the skin friction, together with a lesser effect on the output of the gauges themselves, and this affected the accuracy of the measurements. Thus, it was necessary to take the mean of a number of measurements to obtain reasonable accuracy.

The fuel-on values of skin friction were not significantly different from the fuel-off values, indicating that the mean skin friction was not affected by supersonic combustion in the duct. The fuel-off values and, by implication, the fuel-on values of skin friction were consistent with predictions based on existing theory for turbulent boundary layers.

Measurements of heat transfer rate were also made, and exhibited a relationship to the levels of skin friction that was consistent with Reynolds analogy. This relationship was the same for the fuel-on and fuel-off cases provided that, in the fuel-on case, the effect of combustion on the mainstream properties was taken into account through a Rayleigh analysis.

Because the experiments were performed in a shock tunnel, the surface temperatures were close to the ambient value of 300 K, and the higher surface temperatures that are appropriate to a flight situation might cause the preceding conclusions to be modified. Having noted this caveat, it is also worth observing that the measured values of the skin-friction coefficient are on the low side of estimates that have been made for flows with supersonic combustion, and this is an encouraging sign for the future of air-breathing propulsion at high speeds.

Acknowledgments

The authors are grateful to Christopher Craddock, who performed the computer simulations for Fig. 11. They also are appreciative of the part played by J. Brennan in the developmental manufacture of the skin-friction gauges and of discussions with M. Smart, of NASA Langley Research Center. The shock tunnel was operated under a grant from the Australian Research Council.

References

[1]Paull, A., Stalker, R. J., and Mee, D. J., "Experiments on Supersonic Combustion Ramjet Propulsion in a Shock Tunnel," *Journal of Fluid Mechanics*, Vol. 296, Aug. 1995, pp. 159–183.

[2]Chinitz, W., Erdos, J. J., Rizkalla, O., Anderson, G. Y., and Bushnell, D. M., "Facility Opportunities and Associated Stream Chemistry

Considerations for Hypersonic Air-Breathing Propulsion," *Journal of Propulsion and Power*, Vol. 10, No. 1, 1994, pp. 6–17.

[3]Holden, M. S., "An Experimental Investigation of Turbulent Boundary Layers at High Mach Number and Reynolds Numbers," NASA CR-112147, Nov. 1972.

[4]Goyne, C. P., Paull, A., and Stalker, R. J., "A Skin Friction Gauge for Impulsive Flows," AIAA Paper 95-3152, July 1995.

[5]Goyne, C. P., Paull, A., and Stalker, R. J., "Skin Friction Measurements in the T4 Shock Tunnel," *Proceedings of the 21st International Symposium on Shock Waves*, edited by A. F. P. Houwing, Australian National Univ., Canberra, Australia, 1997, pp. 1125–1130.

[6]Novean, M. G., Schetz, J. A., and Bowersox, R. D. W., "Direct Measurements of Skin Friction in Complex Supersonic Flows," AIAA Paper 97-0394, Jan. 1997.

[7]Bowersox, R. D. W., Schetz, J. A., Chadwick, K., and Deiwert, S., "Technique for Direct Measurement of Skin Friction in High Enthalpy Impulsive Scramjet Flowfields." *AIAA Journal*, Vol. 33, No. 7, 1995, pp. 1286–1291.

[8]Kelly, G. M., Simmons, J. M., and Paull, A., "Skin Friction Gauge for Use in Hypervelocity Impulse Facilities," *AIAA Journal*, Vol. 30, No. 3, 1992, pp. 844, 845.

[9]Jacobs, P. J., and Stalker R. J., "Mach 4 and Mach 8 Axisymmetric Nozzles for a High Enthalpy Shock Tunnel," *Aeronautical Journal of the Royal Aeronautical Society*, Vol. 95, No. 949, 1991, pp. 324–334.

[10]Lordi, J. A., Mates, R. E., and Moselle, J. R., "Computer Program for the Numerical Solution of Nonequilibrium Expansion of Reacting Gas Mixtures," NASA CR-472, May 1966.

[11]Paull, A., "A Simple Shock Tunnel Driver Gas Detector," *Shock Waves Journal*, Vol. 6, No. 5, 1996, pp. 309–312.

[12]Skinner, K. A., and Stalker, R. J., "Species Measurements in a Hypersonic, Hydrogen-Air, Combustion Wake," *Combustion and Flame*, Vol. 106, No. 4, 1996, pp. 478–486.

[13]McIntyre, T. J., Houwing, A. F. P., Palma, P. C., Rabbath, P. A. B., and Fox, J. S., "Optical and Pressure Measurements in Shock Tunnel Testing of a Model Scramjet Combustor," *Journal of Propulsion and Power*, Vol. 13, No. 3, 1997, pp. 388–394.

[14]He, Y., and Morgan, R. G., "Transition of Compressible High Enthalpy Boundary Layer over a Flat Plate," *Aeronautical Journal of the Royal Aeronautical Society*, Vol. 98, No. 972, 1994, pp. 25–34.

[15]Schultz, D. F., and Jones, T. V., "Heat Transfer Measurements in Short-Duration Hypersonic Facilities," *Advisory Group for Aerospace Research and Development*, AGARDograph No. 165, 1973, p. 101.

[16]Smith, C. E., "The Starting Process in a Hypersonic Nozzle," *Journal of Fluid Mechanics*, Vol. 24, Pt. 4, 1966, pp. 625–640.

[17]Winter, K. G., "An Outline of the Techniques Available for the Measurement of Skin Friction in Turbulent Boundary Layers," *Progress in the Aerospace Sciences*, Vol. 18, Pergamon, Oxford, 1977, pp. 1–57.

[18]Spalding, D. B., and Chi, S. W., "The Drag of a Compressible Turbulent Boundary Layer on a Smooth Flat Plate With and Without Heat Transfer," *Journal of Fluid Mechanics*, Vol. 18, Pt. 1, 1964, pp. 117–143.

[19]Craddock, C. S., and Jacobs P. A., "A Space-Marching Compressible Flow Solver with Chemistry and Optimization SM-3D^{plus}," Dept. of Mechanical Engineering, Univ. of Queensland, Brisbane, Australia, June 1998.

[20]White, F. M., *Viscous Fluid Flow*, 2nd ed., McGraw–Hill, New York, 1991.